第33卷 第7期 焊 接 学 报 Vol. 33 No. 7
2012年7月 TRANSACTIONS OF THE CHINA WELDING INSTITUTION July 2012

基于B样条曲线的X射线图像焊缝缺陷分割与提取

梁 硼， 魏艳红， 占小红

（南京航空航天大学 材料科学与技术学院，南京 211100）

梁 硼

摘 要：针对大部分X射线数字图像低对比度、背景起伏大以及纹理复杂的问题，在X射线数字焊缝图像预处理之后，采用B样条曲线对列灰度曲线进行拟合，获得光滑而且顺畅的曲线. 在此基础上进一步提取曲线的极值点，并通过定义的波动阈值以及边界阈值进行两次极值点集合的修正. 最后利用数学形态学及中值滤波对缺陷的形状和大小进行了修正. 结果表明，该技术有效地解决了X射线图像由于焊缝纹理复杂导致缺陷提取困难的问题，有利于实现X射线图像焊接缺陷的自动提取.

关键词：样条曲线；焊接缺陷；图像处理

中图分类号：TG409 **文献标识码**：A **文章编号**：0253-360X(2012)07-0109-04

0 序 言

焊接质量决定着焊接结构件的使用寿命，而检测焊缝内的缺陷又是保证焊接质量的重要手段. 大量焊接结构件采用X射线进行检测，采集到的X射线底片大部分采用人工评定. 人工评定直接影响焊接缺陷评定的客观化、科学化与规范化，因此对于实现焊接缺陷分析与识别的自动化显得尤其重要.

目前，针对X射线图像中焊接缺陷的自动分割与提取许多研究学者进行了相关的研究[1-3]. 其中，图像分割是焊接缺陷提取与识别的关键技术，主要采用的分割方法有阈值分割法、边缘检测法[4]以及列灰度曲线波形分析法. 其中张晓光、Shafeek等人[5,6]利用阈值分割方法对未去除背景的缺陷进行了研究，对于缺陷与背景灰度对比度较大的图像有着良好的分割效果，但是对于灰度分布不均衡的焊缝图像，尤其焊缝边缘灰度接近缺陷灰度，很容易误将焊缝边缘划为焊接缺陷. 孙怡等人[7]提出了一种基于图像空间特性（空间对比度与空间方差）的模糊识别算法，与传统检测方法相比有着较低的误判率及漏判率，但是未涉及焊缝背景、纹理复杂的X射线图像.

针对背景起伏大且纹理复杂的焊缝图像，利用B样条曲线对列灰度曲线进行平滑优化，然后通过对提取的极值集合进行分析，确定焊缝缺陷的边界，实现焊接缺陷的分割与提取.

收稿日期：2011-05-23

1 基于B样条的灰度曲线拟合算法

1.1 焊缝图像的前处理

X射线数字图像采集进计算机后，存在噪声多、对比度低、背景起伏大、焊缝边缘模糊等问题. 所以在缺陷提取之前，需进行图像预处理，去除不必要的图像信息，加快处理速度.

利用焊缝提取以及图像增强等方法进行焊缝图像的预处理. 其中焊缝提取利用了基于灰度投影的方法[8]，图像增强采用了由Pal提出的模糊增强法[9]，处理结果如图1所示.

图1 焊缝图像前处理结果
Fig. 1 Result of image preprocessing

1.2 B样条曲线拟合列灰度曲线

已提取的焊缝图像背景起伏较大，且具有鱼鳞状的纹理. 纹理的复杂性使得图像列灰度曲线产生大量尖峰，普通区域阈值分割容易产生大量的伪缺陷. 针对实际生产中大量的此类X射线图像，采用B样条曲线拟合的方法，对其列灰度曲线进行平滑与优化. B样条曲线是贝兹曲线的一般化，可以通过给定一组控制点而得到一条曲线. 其优点为一部分控制点的调整只改变曲线的局部行为，而不像贝兹曲线改变全局行为. 所以使用B样条曲线能创建

更为精确的几何模型或线条.

取焊缝图像中的第 204 列与第 208 列的像素，如图 2 所示.

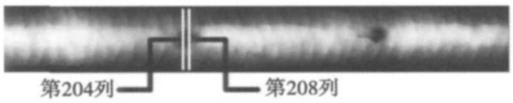

图 2 焊缝图像的第 204 和 208 列像素

Fig. 2 Pixels of row 204 and row 208 of image

根据 B 样条曲线方程定义

$$P(t) = \sum_{i=0}^{n} P_i N_{i,k}(t) \tag{1}$$

式中: $P_i(i=0,1,\cdots,n)$ 为确定 k 阶 B 样条曲线的控制点，即列灰度曲线上离散的点; $N_{i,k}(t)(i=0,1,\cdots,n)$ 为 k 阶 B 样条基函数; $P(t)$ 即为所求曲线.

B 样条曲线拟合的标准算法采用著名的 de Boor-Cox 递推算法，即

$$N_{i1}(t) = \begin{cases} 1, t_i \leqslant x \leqslant t_{i+1} \\ 0, \text{其它} \end{cases} \tag{2}$$

$$N_{i,k}(t) = \frac{t - t_i}{t_{i+k-1} - t_i} N_{i,k-1}(t) + \frac{t_{i+k} - t}{t_{i+k} - t_{i+1}} N_{i+1,k-1}(t) \tag{3}$$

由于列灰度曲线上离散点的间隔为 1 个像素，所以令 $t_{i+1} - t_i = 1, t_0 = 0$.

图 3 为 B 样条曲线拟合后第 204 列与第 208 列像素点的列灰度曲线效果.

与拟合前列灰度曲线相比，尖峰和拐点较少的第 204 列灰度曲线拟合后，保持着原有曲线平滑特征. 对于第 208 列曲线，通过 B 样条曲线的拟合，曲线在大部分尖峰及拐点附近得到了光滑处理.

2 灰度曲线极值点提取及修正

2.1 极值点的提取

列灰度曲线平滑之后，通过极值点集合的提取与修正，可得到曲线中缺陷边界点.

在列灰度曲线中，低于理想焊缝灰度的缺陷分布于曲线低谷位置. 利用一阶差分对曲线进行极值的提取. 具体方法如下.

(1) 将得到的灰度序列曲线离散化，得到曲线的各个点为 (x_1, y_1), $(x_2, y_2)\cdots(x_n, y_n)$，其中 $n \geqslant 2$; x 以及 y 分别为各个点的像素位置和像素值. 记曲线点集合为 $\boldsymbol{C}$.

(2) 通过式(4) 求极值点，即

$$m = (y_i - y_{i-1})(y_i - y_{i+1}) \tag{4}$$

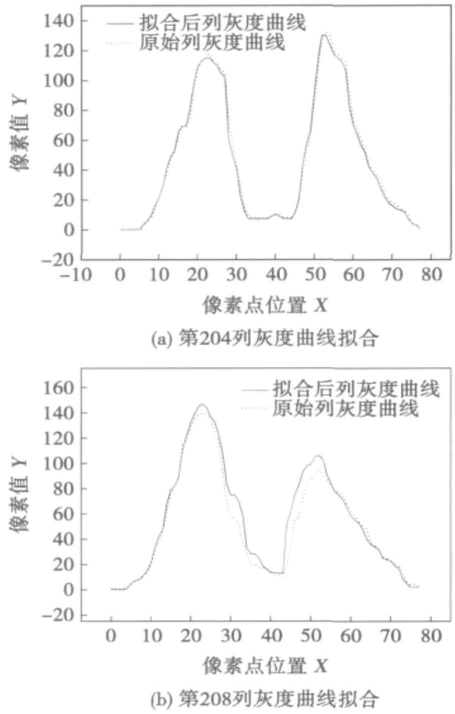

图 3 第 204 列与第 208 列 B 样条曲线拟合结果

Fig. 3 Result of B-spline curve-fitting

式中: y_i 为集合 $\boldsymbol{C}$ 中第 i 个点的像素值. 则当 $m > 0$ 时，所对应的 (x_i, y_i) 为极值点，并将其加入极值点集合 $\boldsymbol{M}$ 中.

第 204 列灰度曲线中的极值点如图 4 所示. 为了后续的计算方便，在所有的极值点中加入曲线的首、末端点.

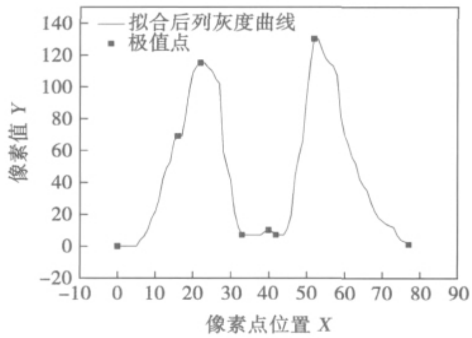

图 4 第 204 列灰度曲线极值点分布

Fig. 4 Extreme value point distribution of row 204

2.2 极值点集合的修正

2.2.1 极值点集合的一次修正

在极值点集合 $\boldsymbol{M}$ 中，部分极值点是无用的或是不利于缺陷边界点的提取. 这些点中包括曲线二阶

差分中的拐点,所以利用下面的公式进行修正.

$$s = (m_i - m_{i-1})(m_i - m_{i+1}) \tag{5}$$

式中:m_i为极值点集合 $\boldsymbol{M}$ 中第 i 个点的像素值. 若 $s > 0$,则保留极值点集合 $\boldsymbol{M}$ 中的第 $\boldsymbol{i}$ 个点. 反之,则舍弃. 修正后的极值点集合记为 $\boldsymbol{S}$.

2.2.2　极值点集合的二次修正

由于纹理的复杂性,曲线部分区域中可能会存在前后波动较小的极值点集合,所以定义了一个波动阈值 β,利用如下公式,即

$$|(q_{i+1} - q_i)/(p_{i+1} - p_i)| < \beta \tag{6}$$

式中:(p_{i+1}, q_{i+1}),(p_i, q_i) 为极值点集合 $\boldsymbol{S}$ 中的第 $i+1$ 个点以及第 i 个点. 若满足上述公式,则从 $\boldsymbol{S}$ 集合中移除(p_i, q_i) 点,保留(p_{i+1}, q_{i+1}). 通过极值二次修正后的极值点分布如图 5 所示. 由图 5 可知,处理后的列灰度曲线只保留了对于缺陷边界提取时有用的极值点.

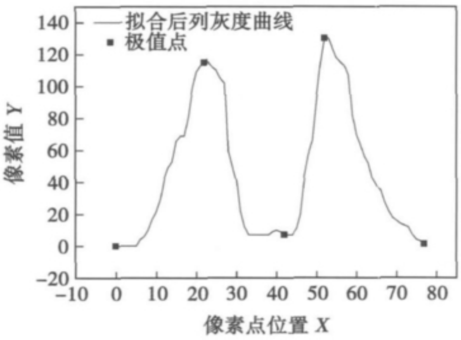

图 5　极值点集合二次修正结果

Fig. 5　Result of second correction

3　焊缝缺陷分割提取及结果

3.1　缺陷边界点的提取

提取出极值点集合之后,可顺利提取出列灰度曲线中缺陷的边界点.

(1) 若集合 $\boldsymbol{S}$ 中点个数大于 3,则定义一个边界阈值 α,利用如下公式,即

$$\mathrm{Min}(z_{i-1}, z_{i+1}) - z_i \geqslant \alpha \tag{7}$$

式中:z_i为极值点集合 $\boldsymbol{S}$ 中第 i 个点的像素值.

(2) 若符合上述公式,则将 $\mathrm{Min}(z_{i-1}, z_{i+1})$ 在集合 $\boldsymbol{S}$ 中对应的点添入缺陷边界点集合,记为 D.

(3) 考察集合 $\boldsymbol{D}$ 中具有最高像素值的两个点,取像素值较低的一个点,记为(a_1, b_1),此为第一个缺陷边界点. 由于集合 $\boldsymbol{C}$ 包含集合 $\boldsymbol{S}$,所以在曲线点集合 $\boldsymbol{C}$ 中寻找从 z_i对应的点到 $\mathrm{Max}(z_{i-1}, z_{i+1})$ 对应的点中像素值最接近 b_1 的另一个缺陷边界点(a_2, b_2).

图 6 是部分常见缺陷在边界阈值 $\alpha = 30$,波动阈值 $\beta = 4$ 时提取后的效果图. 其中包括了三张焊缝纹理复杂的缺陷图像以及一张焊缝纹理简单的缺陷图像.

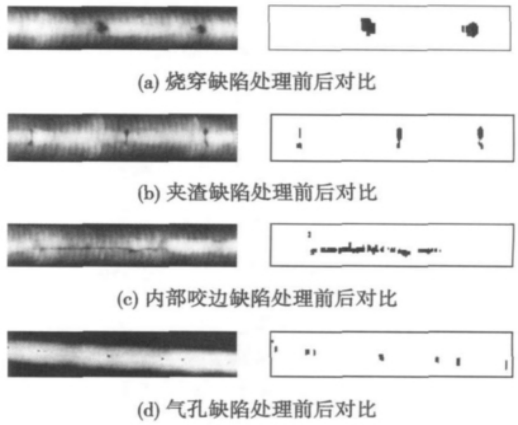

图 6　边界阈值 $\alpha = 30$,波动阈值 $\beta = 4$ 时缺陷提取后的结果

Fig. 6　Result of defect extraction with $\alpha = 30$, $\beta = 4$

由于该方法建立在对焊缝图像列灰度缺曲线分析的基础上,纹理复杂的焊缝图像有着较为不规则的列灰度曲线,但通过设置的边界阈值 α 以及波动阈值 β 能够忽略曲线的不规则性,并准确识别缺陷边界,所以该方法普适性得到了较大的提高.

3.2　缺陷形状大小修正及结果

缺陷提取后,利用数学形态学进行水平方向 1 个像素的膨胀合并细小间隙,并利用 7×7 中值滤波平滑缺陷边界并且剔除极细小的伪缺陷. 缺陷的形状、大小修正后的结果如图 7 所示.

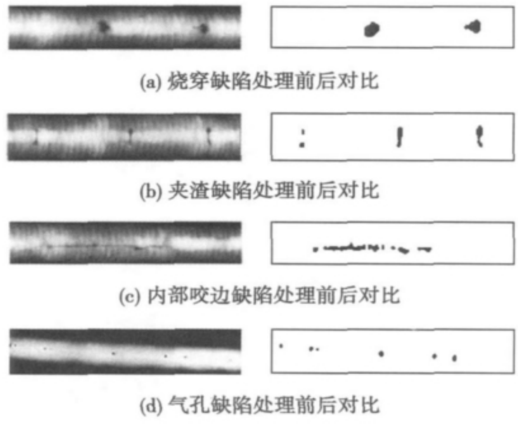

图 7　缺陷形状大小修正后的结果

Fig. 7　Result of shape and size correction

4 结 论

(1) 采用 B 样条曲线对列灰度曲线进行平滑处理,为后续极值正确提取提供了方便.

(2) 利用极值点集合提取以及两次极值点集合修正确定提取缺陷边界点时有用的极值点集合.

(3) 定义边界阈值以及波动阈值确定极值点集合中缺陷边界的点集.

(4) 利用数学形态学和中值滤波来修正缺陷的大小及形状,达到了良好的效果.

参考文献:

[1] 邵家鑫,都 东,朱新杰,等. 基于 X 射线数字化图像处理的双面焊焊缝缺陷检测[J]. 焊接学报,2010,31(11):21-24.
Shao Jiaxin,Du Dong,Zhu Xinjie,*et al*. Weld defect detection of double sides weld based on X-ray digitized image[J]. Transactions of the China Welding Institution,2010,31(11):21-24.

[2] 陈 明,马跃洲,陈 光. X 射线线阵实时成像焊缝缺陷检测方法[J]. 焊接学报,2007,28(6):81-84.
Chen Ming,Ma Yuezhou,Chen Guang. Weld defects detection for X-ray linear array real-time imaging[J]. Transactions of the China Welding Institution,2007,28(6):81-84.

[3] 侯润石,都 东,邵家鑫,等. 基于局部曲面重构的焊缝 X 射线图像缺陷分割技术[J]. 无损检测,2008,30(8):533-535.
Hou Runshi,Du Dong,Shao Jiaxin,*et al*. Background subtraction segmentation of weld defects in X-ray image based on partial surface reconstruction[J]. Nondestructive Testing,2008,30(8):533-535.

[4] 殷晓辉,韩晓微,高 原,等. 焊接缺陷 X 射线自动检测技术研究现状[J]. 电焊机,2007,37(11):28-31.
Yin Xiaohui,Han Xiaowei,Gao Yuan,*et al*. Study on the key technology for automatic detection of weld defect by radiography[J]. Electric Welding Machine,2007,37(11):28-31.

[5] 张晓光,高 顶. 射线检测焊接缺陷的提取和自动识别[M]. 北京:国防工业出版,2004.

[6] Shafeek H I,Gadelmawla E S,Abdel-Shafy A A,*et al*. Assessment of welding defects for gas pipeline radiographs using computer vision[J]. NDT & E International,2004,37(4):291-299.

[7] 孙 怡,孙洪雨,白 鹏,等. X 射线焊缝图像中缺陷的实时检测方法[J]. 焊接学报,2004,25(2):115-118.
Sun Yi,Sun Hongyu,Bai Peng,*et al*. Real-time automatic detection of weld defects in X-ray images[J]. Transactions of the China Welding Institution,2004,25(2):115-118.

[8] Pratt W. K. Digital image processing[M]. New York:John Wiley and Sons,1978.

[9] Pal S K,King R A. One edge detection of X-ray images using fuzzy sets[J]. IEEE Transactions on Pattern Analysis and Machine Intelligence,1983,5(1):69-77.

作者简介: 梁 硼,男,1987 年出生,硕士. 主要从事焊接质量监测与控制及相关研究. 发表论文 2 篇. Email: lpblueice@126.com

通讯作者: 魏艳红,女,教授,博士生导师. Email: yhwei@nuaa.edu.cn

[上接第 108 页]

TC11 一侧的 TMAZ、TC11 一侧的焊缝、TC17 一侧的焊缝和 TC17 一侧的 TMAZ 所组成.

(2) 焊缝区发生了动态再结晶过程,其发生在完全的 β 相转变之后,摩擦停止后在 TC11 与 TC17 原始摩擦界面上形成了初生 β 共生晶粒,且在其内部存在两种不同形貌的 α 相.

(3) 摩擦时间从 1 s 延长至 4 s,焊缝内初生 β 动态再结晶晶粒尺寸从 9.1 μm 增加到 14.3 μm,TC11 一侧 α 相片层宽度从 128 nm 增加到 255 nm.

参考文献:

[1] 胡美娟,刘金合,康文军,等. 电子束局部热处理对 TC4 钛合金焊接接头组织和性能的影响[J]. 焊接学报,2008,29(2):104-107.
Hu Meijuan,Liu Jinhe,Kang Wenjun,*et al*. Effects of local heat treatment by electron beam on microstructure and properties of TC4 titanium alloy welded join[J]. Transactions of the China Welding Institution,2008,29(2):104-107.

[2] 张田仓,李 晶,季亚娟,等. TC4 钛合金线性摩擦焊接头组织和力学性能[J]. 焊接学报,2010,31(2):53-56.
Zhang Tiancang,Li Jing,Ji Yajuan,*et al*. Structure and mechanical properties of linear friction welding joint [J]. Transactions of the China Welding Institution,2010,31(2):53-56.

[3] 马铁军,杨思乾,张 勇,等. TC4 线性摩擦焊接头的力学性能及组织变化特点[J]. 焊接学报,2007,28(10):17-20.
Ma Tiejun,Yang Siqian,Zhang Yong,*et al*. Mechanical properties and microstructure features of linear friction welded TC4 titanium alloy joint [J]. Transactions of the China Welding Institution,2007,28(10):17-20.

[4] Romero J,Attallah M M,Preuss M,*et al*. Effect of the forging pressure on the microstructure and residual stress development in Ti-6Al-4V linear friction welds[J]. Acta Materialia,2009,57:5582-5592.

[5] Karadge M,Preuss M,Lovell C,*et al*. Texture development in Ti-6Al-4V linear friction welds[J]. Materials Science and Engineering A,2007,459:182-191.

作者简介: 郎 波,男,1980 年出生,博士,高级工程师. 主要从事扩散焊、摩擦焊的基础研究与工程应用工作. 发表论文 20 余篇. Email: langbo198009@163.com

ing temperature increasing. It also increased with strain rate decreasing. Average grain size increased with straining, and with forming temperature increasing.

Key words: microstructure evolution; laser welding; superplastic deformation

Microstructure and properties of dissimilar materials Mg/Al laped joint by friction stir welding CHEN Ying, FU Ningning, SHEN Chenbin, GE Jiping (School of Materials Science and Engineering, Dalian Jiaotong University, Dalian 116028, China). pp 93 - 96

Abstract: 5083 aluminum alloy and AZ31 magnesium alloy were lap jointed by using friction stir lap welding. The mechanical properties, microstructure and fracture appearance of the joint were investigated. The results indicated that a high shear strength, interface bonding and defect-free weld have been obtained when the probe of a tool did not contact the lower Mg sheet and the suitable welding parameters are used. 5083 and AZ31 were jointed by a conversion layer that existed in interface zone which contained intermetallic compounds. The joints fractured in interface. Fractographs confirm that the fracture of the Al side is composed of the "small pit" by plastic tearing, but the fracture of the Mg side consists of river line pattern mainly. The micro hardness raised in the interface zone.

Key words: friction stir lap welding; magnesium alloy; aluminum alloy; conversion layer

Microstructure characteristics and properties of steel stud to aluminum alloy made by covering filler metal brazing
GE Jiaqi, JIANG Yong, WANG Kehong (School of Material Science and Engineering, Nanjing University of Science and Technology, Nanjing 210094, China). pp 97 - 100

Abstract: Q235 steel stud and 6061 aluminum alloy with AlSi as filler metal were joined by using high-frequency induction brazing. Microstructure, composition and phase composition of the welded joint were characterized by optical microscopy, SEM, EDAX EDS diffraction analysis. The results showed that AlSi filler completely reacted to 6061 aluminum base metal, needle-like eutectic was formed with the diffusion of Si to aluminum base metal; continuous Fe-Al intermetallic compounds which should be composed of Fe_2Al_5 and $FeAl_3$ generated near the steel side in the brazing seam, and some cellular crystal generated along the direction perpendicular to the Al base metal. Mechanical properties tests showed that the shear strength of welding joint was up to 65 MPa, fracture occurred in the Fe-Al intermetallic compounds where the microhardness was high. Fracture properties belonged to ductile fracture.

Key words: high-frequency induction brazing; dissimilar metal welding; microstructure; intermetallic compounds

Research on laser spot weld-bonding process characteristics
WANG Mingmao[1], TAO Wang[1], MA Yinan[1], CHEN Yanbin[1], WANG Yang[2] (1. State Key Laboratory of Advanced Welding and Joining, Harbin Institute of Technology, Harbin 150001, China; 2. School of Mechatronics Engineering, Harbin Institute of Technology, Harbin 150001, China). pp 101 - 104

Abstract: The stability of the laser spot weld-bond is analyzed and the exhaust means of the gas from the adhesives with different properties are studied. The weld defects of laser spot weld-bonding process are solved. The key of the weld-bonding process is the appropriate exhaust path for the gas from the adhesive decomposition, the plate gap is an important exhaust channel. The greater the adhesive viscosity is, the worse the weldability is. For the low viscosity adhesive, a reliable connection can be got by the slow rising laser pulse welding technology; for the large viscosity adhesive, a reliable connection can be achieved by filler wire and using the laser spike pulse welding process. The welding process can solve the weld defects of different viscosity adhesive, expanding the applications of the laser weld-bonding technology.

Key words: laser spot weld-bond; adhesive layer; viscosity; spatter; pulse

Microstructure in linear friction welded dissimillar titanium alloy joint LANG Bo, ZHANG Tiancang, TAO Jun, GUO Delun (Beijing Aeronautical Manufacturing Technology Research Institute, Beijing 100024, China). pp 105 - 108, 112

Abstract: Microstructure at the different zones of linear friction welded TC11 and TC17 dissimillar titanium alloy joint were investigated to understand the mechanism of microstructural formation in the joints. The results showed that four different structures existed in linear friction welded joint, i. e. thermomechanically affected zone (TMAZ) in the region close to TC11 parent material, TMAZ the region close to TC17 parent material, weld zone in the region close to TC11 TMAZ, and weld zone in the region close to TC17 TMAZ. Although no dynamic recrystallization was observed in the TMAZ, the phase transformation would occur concurrently with material deformation during welding. In contrast, dynamic recrystallization occurred in the weld. Common prior-beta grains were formed at the original rubbing interface after welding. Under the conditions of 3 mm amplitude of oscillation, 40 Hz frequency of oscillation, 66.7 MPa friction pressure and absence of forge force, prior-beta grain size and alpha plate width increased with friction time increasing.

Key words: titanium alloy; linear friction welding; microstructure

Weld defect segmentation and extraction of X-ray image based on B-spline curve LIANG Peng, WEI Yanhong, ZHAN Xiaohong (College of Material Science and Technology, Nanjing University of Aeronautics and Astronautics, Nanjing 211100, China). pp 109 - 112

Abstract: Aiming at the facts that most X-ray digital images have the problem of low contrast, large background fluctuation and complex texture, b-spline curve is used to fit the column gray curves after preprocessing of weld images. The result shows that redundant curve peaks are eliminated and a smooth curve is abtained. Furthermore, curve extreme points are extracted and extreme value point set is modified twice by a fluctuation threshold and a boundary threshold. Finally, the shape and size of defects are revised by mathematical morphology and median filtering. Experiment results shows that this strategy effectively solves the problem of defect extraction caused by the weld seam with complex texture in X-ray image. It is advantageous to realize the automatic extraction of weld defects in X-ray image.

Key words: spline curve; weld defect; image processing